Article

Optimal Parameter Identification of Perovskite Solar Cells Using Modified Bald Eagle Search Optimization Algorithm

Abdul Ghani Olabi [1,2,*], Hegazy Rezk [3,4], Mohammad Ali Abdelkareem [1,5,*], Tabbi Awotwe [2], Hussein M. Maghrabie [6], Fatahallah Freig Selim [7], Shek Mohammod Atiqure Rahman [1], Sheikh Khaleduzzaman Shah [8,*] and Alaa A. Zaky [7]

1   Sustainable Energy & Power Systems Research Centre, RISE, University of Sharjah, Sharjah P.O. Box 27272, United Arab Emirates
2   Mechanical Engineering and Design, School of Engineering and Applied Science, Aston University, Aston Triangle, Birmingham B4 7ET, UK
3   Department of Electrical Engineering, College of Engineering in Wadi Alddawasir, Prince Sattam bin Abdulaziz University, Wadi Alddawasir 11991, Saudi Arabia
4   Electrical Engineering Department, Faculty of Engineering, Minia University, Minia 61111, Egypt
5   Chemical Engineering Department, Faculty of Engineering, Minia University, Minia 61111, Egypt
6   Department of Mechanical Engineering, Faculty of Engineering, South Valley University, Qena 83521, Egypt
7   Electrical Engineering Department, Kafrelsheikh University, Kafrel-Sheikh 33511, Egypt
8   Renewable Energy and Energy Efficiency Group, Department of Infrastructure Engineering, Faculty of Engineering and Information Technology, The University of Melbourne, Parkville, VIC 3010, Australia
*   Correspondence: aolabi@sharjah.ac.ae (A.G.O.); mabdulkareem@sharjah.ac.ae (M.A.A.); sheikhkhaleduzzaman.shah@unimelb.edu.au (S.K.S.)

Abstract: In this paper, a modified bald eagle search optimization algorithm was applied for the first time to determine the parameters of the triple diode model (TDM) of perovskite solar cells (PSCs). Two experimental datasets are considered; the first is measured I–V points for a PSC at standard conditions. The second consists of the measured I–V points for a modified PSC. In contrast, the cost function to be minimized is the root mean square error (RMSE) between the experimental dataset and the calculated one. To prove the superiority of modified bald eagle search optimization (mBES), a comparison with the original bald eagle search optimization (BES), particle swarm optimizer (PSO), Hunger games search (HGS), and recent Coronavirus Disease Optimization Algorithm (COVIDOA) was implemented. Furthermore, statistical analysis of ANOVA and Tukey tests was performed. The results demonstrate the lead of the recommended mBES in identifying the parameters of the TDM for PSCs, where the RMSE achieved the least value among the used optimization algorithms in this study.

Keywords: perovskite solar cell; triple diode model; bald eagle search

1. Introduction

Due to the increasing power demand and negative impact of conventional primary energy sources, such as fossil fuels [1,2], sustainable and clean energy, such as renewable energy sources, must be developed and deployed [3,4]. Nowadays, solar energy is the most promising renewable energy source, and its deployment has rapidly increased around the globe. Sunlight is turned into energy in solar photovoltaic power-producing systems. Additionally, deploying solar technology would significantly lessen problems related to energy security, climate change, unemployment, and other challenges [5].

Perovskite materials are particularly effective solution-processed materials in photovoltaic (PV) manufacturing because of their characteristics, such as strong absorption and extended diffusion length. Therefore, Perovskite solar cells (PSCs), a subset of 3rd generation solar cells, are produced due to the employment of perovskite materials. Within just a few years of improvement, PSCs power conversion efficiency (PCE) reached 25.5% [6]. This

rapid increase in PCE makes PSCs an excellent alternative to silicon-based PV technology. However, a fundamental barrier to their widespread commercialization is the PSC stability issue, which must be resolved [7–9]. Researchers have suggested some methods for improving PSCs' PCE and resolving their stability issues. Dimensionality optimization [8,10] employs a stable organic cation in forming perovskite material, and interface engineering [11,12] is among the strategies that have played an essential role in improving stability and efficiency. Problems of hysteresis [13,14] in PSCs and perovskite degradation [15,16] can be resolved using interface engineering [11,17].

Authors in [18–21] investigated an optimized design of different types of perovskite solar cell via SCAPS-1D, DFT, and wxAMPS software packages where many electron transport layers were used and examined beside the interface between the electron transporting layer and the perovskite absorber layer.

In literature, rare earth oxides are used in the PSCs performance improvement [22]. In [23], a review paper, the authors discussed the recent development in the proton-conducting performance of BaZrO3 as standpoint energy materials to integrate the fundamental knowledge of proton-conducting BZO perovskites.

Perovskite absorbers modified with organic molecules have received much attention. This is due to their easy processability and acceptable electronic characteristics of the organic molecules. Electrical modeling of the whole perovskite solar cell device is required to evaluate PSC performance better. Device properties like the current at a short circuit, the voltage at an open circuit, fill factor, diode ideality factor, series, shunt resistances, and efficiency may be easily measured and adjusted using an electrical model [17,24,25]. One of the most frequent methods to characterize the performance of a PV cell and module is through its relation between the current and the voltage. This relation can provide simple information such as the voltage at open circuit and the current at short circuit conditions, and the power at the point of maximum power. Even PV module makers must disclose that essential information is evaluated under defined test settings (STC). Extracting further information from the I–V curves is challenging without the assistance of mathematical models. Because the I–V curves of a PV system contain a significant degree of nonlinearity, the optimal design is challenging.

According to the literature, there are three standard models for solar cell performance: one diode, two diodes, and triple diode models. The main components in these models are the diodes and the attached resistors. The main parameters optimal value has to be determined to successfully model a solar cell. These parameters are the diode ideality factor, series and parallel resistors, and the diode saturation current. The first model for solar cell modeling is the single diode model; however, it has some drawbacks. Due to these drawbacks, more open models with more details are needed as a result. The double and triple-diode models appeared to cover the solar cell performance under different conditions.

The increased installation and penetration of large-scale PV arrays need accurate characterization models, particularly during low solar radiation circumstances, for devising control methods for integrating PV systems to assure the power system stability. Due to including the effect of grain boundaries, leakage current, and the recombination of carriers, the triple diode model is the best model for simulating the solar cell performance [26].

Recently, the modeling, parameters estimation, and application in real systems of the third-generation solar cells, including PSCs, were discussed in a few publications [27–31]. Much research is still required to enhance the parameters estimation problem quality via the mathematical model and the recent bioinspired optimization algorithms [32–38].

Here, the triple diode model was investigated for PSCs performance simulation and modeling and solved via the modified bald eagle search (mBES) algorithm. The original BED provides its ability for many optimization and engineering issues. The mBES is an updated version with additional features for enhancing its performance compared to the BES. For this end, the mBES was chosen. In this work, two datasets of lab-fabricated PSCs devices (control and modified device) were used, as explained in detail in [39]. To prove

the superiority of mBES, a comparison with the original BES, particle swarm optimizer (PSO), Hunger games search (HGS), recent Coronavirus Disease Optimization Algorithm (COVIDOA), and bald eagle search algorithm (BES) was conducted.

The contribution of the work can be outlined as follows.

For the first time, a modified bald eagle search algorithm has been applied to determine the optimal parameters of TDM of perovskite solar cells.

The attained outcomes by mBES are compared with recent algorithms.

The precision and superiority of mBES in identifying the parameters of the TDM are demonstrated.

The rest of the paper is structured as follows: Section 2 briefly summarizes the experimental datasets. The problem construction is explained in Section 3. A brief summary of the modified BES is given in Section 4. The discussion of the results is conducted in Section 5. Finally, Section 6 gives the conclusion of this paper.

2. Experimental Datasets

Two experimental datasets are considered; the first is measured I–V points for a PSC at standard conditions. For both datasets, the test was performed at standard conditions (25 °C, 1000 W/m^2). The number of points was 426 for both PSCs, as shown in Figure 1. Table 1 presents the general data related to the datasets. Both the control and modified devices were fabricated, as explained in reference [39]. In brief, the control device was fabricated based on the spin coating technique where the device layers were deposited as follows. Firstly, the FTO glass substrate was etched and cleaned. The titania electron transporting layer was deposited after that, in a glove box, where both the perovskite and the hole-transporting (Spiro-OMeTAD) layers were deposited. Finally, the silver electrodes were deposited via the thermal evaporation method. For the modified device, the same steps and the electron transporting layer were modified via applying porphyrin over it before depositing the perovskite layer for electron movement facilitation and grain boundary-reducing.
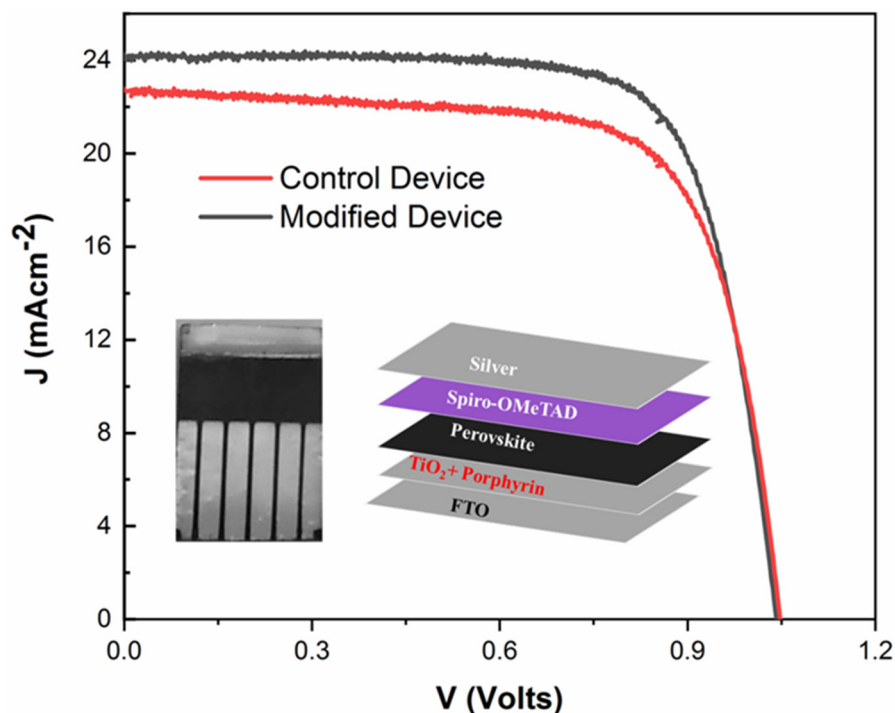

Figure 1. Current density–voltage curves of control and modified PSCs with device structure (inset).

Table 1. General data related to control and modified PSCs.

Parameter	Type of PSC	
	Control	Modified
Number of samples	426	426
Test Temperature, C	25	25
Test radiation, W/m^2	1000	1000
Short circuit current, mA/cm^2	22.6	24.0
Open circuit voltage, V	1.04	1.04
Current at MPP, mA/cm^2	19.88	22.59
Voltage at MPP, V	0.853	0.826
Maximum power, W	16.96	18.67

3. Problem Formulation

In this section, the mathematical representation of the triple diode model proposed for the performance simulation of perovskite solar cells is presented and investigated. The electrical correspondent circuit of the triple diode model is displayed in Figure 2.
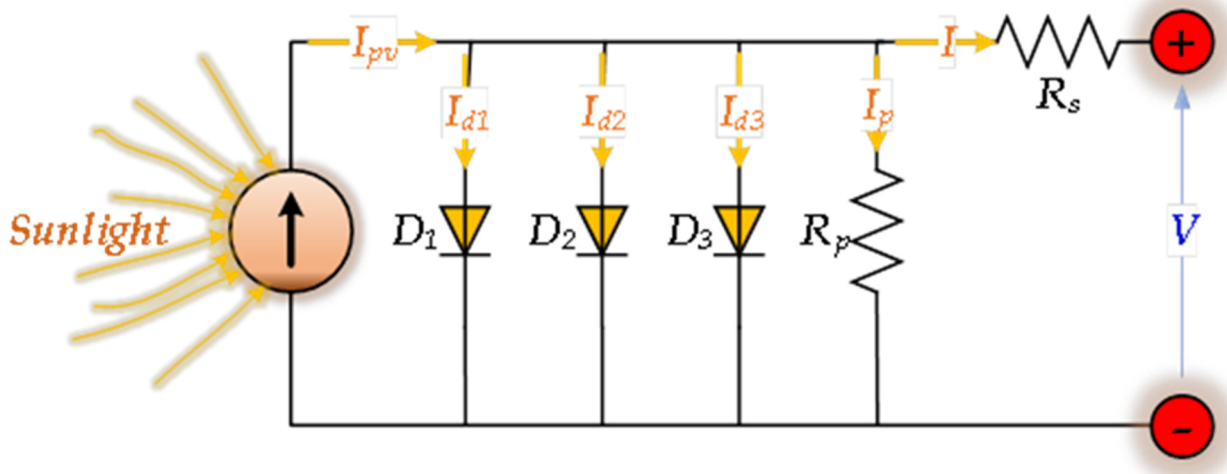
Figure 2. TDM of a solar cell.

From Figure 2, the output current of the solar cell can be estimated by the subsequent relation:

$$I = I_{pv} - I_{D1} - I_{D2} - I_{D3} - \left(\frac{V + I \cdot R_s}{R_p}\right) \tag{1}$$

where I_{pv} depicts the current generated from photons. I_{D1}, I_{D2}, and I_{D3} represent the current in diode 1, diode 2, and diode 3, correspondingly. R_s indicates the series resistance. R_p symbolizes the shun resistance. Based on the Shockley formula, the current through diodes can be formulated as follows:

$$\begin{aligned}
I_{D1} &= I_{01}(e^{\left(\frac{V + I \cdot R_s}{n_1 \cdot V_t}\right)} - 1) \\
I_{D2} &= I_{02}(e^{\left(\frac{V + I \cdot R_s}{n_2 \cdot V_t}\right)} - 1) \\
I_{D3} &= I_{03}(e^{\left(\frac{V + I \cdot R_s}{n_3 \cdot V_t}\right)} - 1)
\end{aligned} \tag{2}$$

where n_1, n_2, and n_3 signify the first, second, and third diode ideality factor, correspondingly; I_{01}, I_{02} and I_{03} are the currents at saturation of diode 1, diode 2, and diode 3, correspondingly. V_t designates the thermal voltage. It can be considered via the following equation:

$$V_t = \frac{kTN_s}{q} \tag{3}$$

where k symbolizes the Boltzmann constant. T is the PV panel temperature. N_s indicates the number of series solar cells, and q symbolizes the electron's charge. Based on the relation mentioned above, the solar cell output current considering TDM can be estimated as follows:

$$I = I_{pv} - I_{01}(e^{(\frac{V+I \cdot R_s}{n_1 \cdot V_t})} - 1) - I_{02}(e^{(\frac{V+I \cdot R_s}{n_2 \cdot V_t})} - 1) - I_{03}(e^{(\frac{V+I \cdot R_s}{n_3 \cdot V_t})} - 1) - \frac{V + I \cdot R_s}{R_p} \tag{4}$$

To increase the current and voltage of the PV array, the solar devices are connected in series and parallel combinations. Therefore, considering the number of parallel strings (N_p) and a number of series cells (N_s), the PV output current, I, is described as:

$$I = N_p \left[I_{pv} - I_{01}(e^{(\frac{\frac{V}{N_s} + \frac{I \cdot R_s}{N_p}}{n_1 \cdot V_t})} - 1) - I_{02}(e^{(\frac{\frac{V}{N_s} + \frac{I \cdot R_s}{N_p}}{n_2 \cdot V_t})} - 1) - I_{03}(e^{(\frac{\frac{V}{N_s} + \frac{I \cdot R_s}{N_p}}{n_3 \cdot V_t})} - 1) \right] - \frac{\frac{V N_p}{N_s} + I \cdot R_s}{R_p} \tag{5}$$

Considering Equation (5), the triple diode model encloses nine unknown parameters (I_{pv}, I_{01}, I_{02}, I_{03}, n_1, n_1, n_1, R_s, R_p). Therefore, accurate values of the unknown parameters must be assessed to get the precise characteristics of the solar PV module. The nine unknown parameters of TDM are required to be identified accurately. The RMSE is estimated using the relation:

$$\text{RMSE} = \sqrt{\frac{1}{N} \sum_{i=1}^{N} (I_m - I_e)^2} \tag{6}$$

where N means the number of datasets, I_m symbolizes the measured current, and I_e designates the assessed current. The RMSE helped assess the optimizers' performance in terms of accuracy (final results accuracy) since it generated smaller fitness values.

4. The Modified Bald Eagle Optimization Algorithm

In this study, the mBES algorithm was employed [40]. The mBES is based on changing the control factors that regulate location change in each iteration from constant parameters to variables whose values vary depending on the iteration. Furthermore, to improve its exploration and exploitation process, the mBES enhances the influence of this parameter as a function of the maximum number of iterations and the actual iteration. As a result, there was higher performance. This algorithm has three phases, as follows.

(a) Phase selection: the eagle searches for a new place close to its optimum position. However, as the number of iterations rises, the gap between the best and new places decreases. This phase may be expressed as follows

$$P = P_{best} + TF \cdot r \cdot (P_m - P) \tag{7}$$

where P_m denotes the mean of all positions, and TF is an adaptive parameter called transition factor used to improve the exploitation and exploration phases. It can be formulated as

$$TF(i) = k(1 + \frac{I_{\max} - i}{I_{\max} + i}) \tag{8}$$

where $I_{\max}$ expresses the maximum number of iterations, i is the current iteration, and k is a gain [1.5, 2].

(b) Searching phase: the eagle searches and updates its position in this phase as follows

$$P^j = P^j + y^j \cdot (P^j - P^{j+1}) + x^j \cdot (P^j - P_m) \tag{9}$$

where P^j is the jth new position, and x and y are the directional coordinate indicators that can be obtained as follows

$$\begin{cases} x^j = \frac{xr^j}{\max(|xr|)}; \ xr^j = r^j \cdot \sin(\theta(i)) \\ y^j = \frac{yr^j}{\max(|yr|)}; \ yr^j = r^j \cdot cos(\theta(i)) \\ \theta = C_1 \cdot \pi \cdot rand; \ r = \theta \cdot R \end{cases} \tag{10}$$

where R is a constant [0.5, 2] and C_1 is a control gain that can be obtained as follows

$$C_1 = \alpha_1 (1 + \frac{T_{\max} - t}{T_{\max} + t}) \tag{11}$$

where α_1 is a constant [5,10].

(c) Swooping: this is the last step, where the eagle beats its prey. It can be modeled as follows

$$P^j = rand \cdot P_{best} + x1^j \cdot (P^j - c_1 \cdot P_m) + y1^j \cdot (P^j - EO \cdot P_{best}) \tag{12}$$

where c_1 is a random number [1,2] used to accelerate the eagle's movement, $x1$ and $y1$ are directional coordinate indicators defined in Equation (7), and EO is an enhancement operator used to improve the eagle's movement throughout this phase. This parameter can be defined in Equation (8).

$$\begin{cases} x1^j = \frac{xr^j}{\max(|xr|)}; \ xr^j = r^j \cdot \sin(\theta(i)) \\ y1^j = \frac{yr^j}{\max(|yr|)}; \ yr^j = r^j \cdot cos(\theta(i)) \\ \theta = C_2 \cdot \pi \cdot rand; \ r = \theta \cdot R \end{cases} \tag{13}$$

$$EO = 2 + \sin(2.5 + \frac{i}{I_{\max}}) \tag{14}$$

where C_2 represents a control parameter [5, 10].

5. Results and Discussion

For fair judgment, the population numbers (25) and the iteration numbers (100) were kept the same for all used optimizers in this study. During the optimization process, the RMSE between the experimental datasets and the calculated current density of PSC was used as an objective function, which was to be minimized. The minimum and maximum limits of PSC parameters and the best parameters of two types of PSCs using different optimizers are shown in Table 2. To prove the trustworthiness of the recommended mBES, the considered algorithms were executed 30 times. The statistical assessment of the considered algorithms is shown in Table 3. The details of 30 runs are shown in Table 4. From Table 2, the estimated control and modified device parameters are in agreement with their experimental analogy at very low deviation values. It is unblemished that the recommended optimization tool helped in obtaining the superlative results between all the used optimization tools. It is well-known that both the ideality factor and the current at saturation of the diode are essential elements to study and analyze the PSC performance, but it is complicated to determine them experimentally. Therefore, the simulation model and the proposed optimization tool determined their value. Thus, better understanding and performance of PSC can be performed, and this is also a merit of the simulation used in this study.

Table 3 presents the statistical performance evaluation of the different algorithms, while Table 4 presents the details of this performance. From Table 3, the recommended tool has superiority in both studied cases. Additionally, it indicates that the recommended tool performance is the best among all the tools used in this study. It is also noticed from Table 3 that the mean RMSE values for the control device change between 4.11×10^{-5} and

8.33×10^{-3}. It is clear that the minimum value (4.11×10^{-5}) is obtained by the proposed algorithm, followed by (6.14×10^{-5}) obtained via HGS optimization algorithm. The minimum cost function of 9.22×10^{-6} was achieved by the proposed mBES optimizer tracked by BES and HGS optimizers correspondingly. Concerning the modified devices, the mean RMSE values change between 4.74×10^{-5} and 9.84×10^{-5}. The minimum mean RMSE of 4.74×10^{-5} was attained by the proposed mBES algorithm, followed by 8.70×10^{-5} using the HGS algorithm. The minimum cost function of 1.91×10^{-5} was achieved by the proposed mBES optimizer tailed by the BES and HGS optimizers correspondingly.

Table 2. Best parameter values of PSCs using different algorithms.

Parameter	Limit		Algorithms				
	Min	Max	PSO	HGS	COVIDOA	BES	mBES
			Control solar cell				
I_{sc} (A)	1.0×10^{-3}	5.0×10^{-3}	2.37×10^{-3}	2.28×10^{-3}	2.00×10^{-3}	2.28×10^{-3}	2.28×10^{-3}
I_{o1} (A)	1.0×10^{-20}	5.0×10^{-5}	1.00×10^{-20}	1.00×10^{-20}	1.00×10^{-20}	1.00×10^{-20}	1.00×10^{-20}
I_{o2} (A)	1.0×10^{-20}	5.0×10^{-5}	1.00×10^{-20}	1.00×10^{-20}	1.00×10^{-20}	9.04×10^{-9}	3.42×10^{-11}
I_{o3} (A)	1.0×10^{-20}	5.0×10^{-5}	1.00×10^{-20}	2.89×10^{-8}	1.00×10^{-20}	1.00×10^{-20}	7.60×10^{-9}
α_1	1.0	3.0	3	1.009586	3	3	2.328537
α_2	1.0	5.0	4.681298	1.804456	3.910555	3.34415	2.247224
α_3	1.0	5.0	4.556172	3.757859	1	1.016789	3.598358
R_s	5.00	17.00	17	16.99955	17	16.96838	12.85587
R_P	1000	800	1732.13	8000	5698.447	8000	7704.722
RMSE			3.03×10^{-5}	1.94×10^{-5}	2.63×10^{-4}	1.20×10^{-5}	9.22×10^{-6}
			Modified solar cell				
I_{sc} (A)	1.0×10^{-3}	5.0×10^{-3}	2.52×10^{-3}	2.47×10^{-3}	2.00×10^{-3}	2.46×10^{-3}	2.46×10^{-3}
I_{o1} (A)	1.0×10^{-20}	5.0×10^{-5}	1.00×10^{-20}	1.00×10^{-20}	1.00×10^{-20}	1.88×10^{-10}	1.00×10^{-20}
I_{o2} (A)	1.0×10^{-20}	5.0×10^{-5}	3.74×10^{-7}	1.00×10^{-20}	1.00×10^{-20}	1.00×10^{-20}	1.47×10^{-10}
I_{o3} (A)	1.0×10^{-20}	5.0×10^{-5}	1.00×10^{-20}	1.28×10^{-8}	1.00×10^{-20}	1.00×10^{-20}	1.00×10^{-20}
α_1	1.0	3.0	3	1	3	2.411884	1.113051
α_2	1.0	5.0	5	1.416711	5	1.14972	2.38629
α_3	1.0	5.0	1	3.440509	5	3.697739	1.071518
R_s	5.00	17.00	17	17	17	10.71667	14.60816
R_P	1000	800	6312.055	8000	7900.147	8000	7993.609
RMSE			6.92×10^{-5}	3.58×10^{-5}	5.25×10^{-4}	2.06×10^{-5}	1.91×10^{-5}

Table 3. Statistical performance evaluation of different algorithms (30 times).

	PSO	HGS	COVIDOA	BES	mBES
			Control solar cell		
Best	3.03×10^{-4}	1.94×10^{-5}	2.63×10^{-4}	1.20×10^{-5}	9.22×10^{-6}
Worst	1.11×10^{-2}	8.82×10^{-5}	3.22×10^{-3}	2.63×10^{-4}	8.74×10^{-5}
Average	8.33×10^{-3}	6.14×10^{-5}	1.06×10^{-3}	1.19×10^{-4}	4.11×10^{-5}
Variance	1.40×10^{-5}	6.63×10^{-10}	5.39×10^{-7}	6.43×10^{-9}	1.26×10^{-9}
Median	1.11×10^{-2}	5.83×10^{-5}	7.65×10^{-4}	1.11×10^{-4}	1.43×10^{-5}
STD	3.74×10^{-3}	2.58×10^{-5}	7.34×10^{-4}	8.02×10^{-5}	3.56×10^{-5}
Elasped time					
			Modified solar cell		
Best	6.92×10^{-5}	3.58×10^{-5}	5.25×10^{-4}	2.06×10^{-5}	1.91×10^{-5}
Worst	1.12×10^{-2}	1.49×10^{-4}	3.25×10^{-3}	4.14×10^{-4}	1.02×10^{-4}
Average	9.84×10^{-3}	8.70×10^{-5}	1.23×10^{-3}	1.27×10^{-4}	4.74×10^{-5}
Variance	9.72×10^{-6}	7.25×10^{-10}	4.34×10^{-7}	1.64×10^{-8}	1.31×10^{-9}
Median	1.12×10^{-2}	1.02×10^{-4}	9.43×10^{-4}	8.38×10^{-5}	2.47×10^{-5}
STD	3.12×10^{-3}	2.69×10^{-5}	6.59×10^{-4}	1.28×10^{-4}	3.61×10^{-5}
Elasped time					

Table 4. Details of 30 runs applying different algorithms.

	Control					Modified				
	PSO	HGS	COVIDOA	BES	mBES	PSO	HGS	COVIDOA	BES	mBES
1	1.11×10^{-2}	3.66×10^{-5}	7.65×10^{-4}	1.11×10^{-4}	1.05×10^{-5}	1.12×10^{-2}	1.02×10^{-4}	9.56×10^{-4}	2.03×10^{-4}	2.00×10^{-5}
2	1.11×10^{-2}	8.77×10^{-5}	9.06×10^{-4}	1.60×10^{-4}	8.71×10^{-5}	4.11×10^{-3}	1.02×10^{-4}	8.40×10^{-4}	2.55×10^{-5}	1.91×10^{-5}
3	1.11×10^{-2}	3.56×10^{-5}	9.23×10^{-4}	2.63×10^{-4}	8.74×10^{-5}	1.12×10^{-2}	1.02×10^{-4}	1.69×10^{-3}	4.83×10^{-5}	2.04×10^{-5}
4	1.11×10^{-2}	8.73×10^{-5}	7.65×10^{-4}	8.75×10^{-5}	1.39×10^{-5}	2.72×10^{-3}	7.70×10^{-5}	7.92×10^{-4}	1.73×10^{-4}	1.02×10^{-4}
5	4.08×10^{-3}	3.18×10^{-5}	2.37×10^{-3}	2.36×10^{-4}	1.16×10^{-5}	1.12×10^{-2}	1.03×10^{-4}	1.45×10^{-3}	1.02×10^{-4}	2.40×10^{-5}
6	1.11×10^{-2}	5.69×10^{-5}	1.22×10^{-3}	1.83×10^{-4}	8.74×10^{-5}	1.12×10^{-2}	1.02×10^{-4}	8.41×10^{-4}	2.84×10^{-5}	1.02×10^{-4}
7	1.11×10^{-2}	3.31×10^{-5}	6.59×10^{-4}	1.28×10^{-5}	7.42×10^{-5}	1.12×10^{-2}	1.03×10^{-4}	2.82×10^{-3}	2.06×10^{-5}	1.02×10^{-4}
8	1.11×10^{-2}	2.59×10^{-5}	5.49×10^{-4}	1.20×10^{-5}	9.22×10^{-6}	1.12×10^{-2}	1.02×10^{-4}	8.30×10^{-4}	1.73×10^{-4}	1.94×10^{-5}
9	1.11×10^{-2}	8.82×10^{-5}	3.91×10^{-4}	1.28×10^{-4}	1.13×10^{-5}	1.12×10^{-2}	5.17×10^{-5}	3.25×10^{-3}	1.73×10^{-4}	2.14×10^{-5}
10	1.11×10^{-2}	8.80×10^{-5}	2.91×10^{-4}	1.75×10^{-4}	8.71×10^{-5}	4.11×10^{-3}	1.02×10^{-4}	8.25×10^{-4}	2.50×10^{-5}	2.46×10^{-5}
11	2.74×10^{-3}	3.34×10^{-5}	1.13×10^{-3}	2.51×10^{-5}	1.48×10^{-5}	1.12×10^{-2}	1.02×10^{-4}	8.40×10^{-4}	1.09×10^{-4}	2.06×10^{-5}
12	1.11×10^{-2}	8.75×10^{-5}	6.52×10^{-4}	8.80×10^{-5}	8.71×10^{-5}	1.12×10^{-2}	1.02×10^{-4}	8.41×10^{-4}	4.12×10^{-4}	2.24×10^{-5}
13	4.08×10^{-3}	5.06×10^{-5}	2.58×10^{-3}	1.41×10^{-5}	1.31×10^{-5}	1.12×10^{-2}	5.36×10^{-5}	8.41×10^{-4}	4.11×10^{-4}	1.02×10^{-4}
14	3.03×10^{-4}	5.96×10^{-5}	4.88×10^{-4}	1.25×10^{-5}	9.23×10^{-6}	6.92×10^{-5}	5.19×10^{-5}	1.93×10^{-3}	3.19×10^{-5}	2.13×10^{-5}
15	2.74×10^{-3}	8.77×10^{-5}	7.59×10^{-4}	2.38×10^{-4}	9.24×10^{-6}	1.12×10^{-2}	1.49×10^{-4}	8.26×10^{-4}	4.11×10^{-4}	2.31×10^{-5}
16	1.11×10^{-2}	8.79×10^{-5}	3.22×10^{-3}	1.51×10^{-5}	1.10×10^{-5}	1.12×10^{-2}	4.14×10^{-5}	1.55×10^{-3}	6.79×10^{-5}	1.02×10^{-4}
17	4.08×10^{-3}	8.81×10^{-5}	2.45×10^{-3}	1.82×10^{-4}	1.23×10^{-5}	1.12×10^{-2}	1.02×10^{-4}	1.18×10^{-3}	2.11×10^{-5}	2.88×10^{-5}
18	4.08×10^{-3}	8.79×10^{-5}	3.04×10^{-4}	2.01×10^{-4}	8.72×10^{-5}	1.12×10^{-2}	1.02×10^{-4}	9.33×10^{-4}	2.63×10^{-5}	2.23×10^{-5}
19	4.08×10^{-3}	5.18×10^{-5}	1.17×10^{-3}	2.50×10^{-5}	8.71×10^{-5}	1.12×10^{-2}	4.51×10^{-5}	8.41×10^{-4}	2.13×10^{-4}	2.34×10^{-5}
20	1.11×10^{-2}	4.32×10^{-5}	4.29×10^{-4}	1.28×10^{-5}	8.72×10^{-5}	1.12×10^{-2}	5.33×10^{-5}	1.26×10^{-3}	1.02×10^{-4}	1.02×10^{-4}
21	1.11×10^{-2}	3.19×10^{-5}	7.49×10^{-4}	1.38×10^{-5}	9.73×10^{-6}	1.12×10^{-2}	5.46×10^{-5}	9.54×10^{-4}	3.28×10^{-5}	1.02×10^{-4}
22	1.11×10^{-2}	8.71×10^{-5}	1.24×10^{-3}	9.16×10^{-5}	6.24×10^{-5}	1.12×10^{-2}	1.03×10^{-4}	1.76×10^{-3}	3.41×10^{-5}	2.60×10^{-5}
23	4.08×10^{-3}	8.71×10^{-5}	9.61×10^{-4}	6.97×10^{-5}	2.87×10^{-5}	1.12×10^{-2}	1.03×10^{-4}	8.06×10^{-4}	1.02×10^{-4}	2.42×10^{-5}
24	1.11×10^{-2}	3.78×10^{-5}	1.65×10^{-3}	2.49×10^{-5}	9.72×10^{-6}	1.12×10^{-2}	3.58×10^{-5}	5.25×10^{-4}	5.69×10^{-5}	1.02×10^{-4}
25	1.11×10^{-2}	8.72×10^{-5}	2.63×10^{-4}	1.11×10^{-4}	1.07×10^{-5}	1.12×10^{-2}	1.02×10^{-4}	8.41×10^{-4}	2.22×10^{-5}	3.05×10^{-5}
26	4.08×10^{-3}	3.39×10^{-5}	1.75×10^{-3}	1.85×10^{-4}	8.71×10^{-5}	1.12×10^{-2}	5.38×10^{-5}	9.70×10^{-4}	4.14×10^{-4}	3.28×10^{-5}
27	1.11×10^{-2}	1.94×10^{-5}	6.59×10^{-4}	8.79×10^{-5}	1.27×10^{-5}	1.12×10^{-2}	1.02×10^{-4}	1.04×10^{-3}	9.98×10^{-5}	1.02×10^{-4}
28	1.11×10^{-2}	3.35×10^{-5}	1.28×10^{-3}	8.60×10^{-5}	1.07×10^{-5}	4.11×10^{-3}	1.02×10^{-4}	8.41×10^{-4}	2.41×10^{-5}	2.66×10^{-5}
29	4.08×10^{-3}	8.76×10^{-5}	6.59×10^{-4}	2.36×10^{-4}	1.55×10^{-5}	1.12×10^{-2}	1.02×10^{-4}	9.65×10^{-4}	2.24×10^{-5}	2.41×10^{-5}
30	1.11×10^{-2}	8.70×10^{-5}	4.77×10^{-4}	2.71×10^{-5}	8.74×10^{-5}	1.12×10^{-2}	1.03×10^{-4}	2.74×10^{-3}	3.44×10^{-5}	2.48×10^{-5}

The comparison between the measured datasets and calculated current–voltage and power–voltage for the two studied cases in this work are presented in Figures 3 and 4. The assessment showed that the measured datasets and calculated current–voltage and power–voltage curves are practically matching, which is a sign of the effectiveness of mBES in determining the parameters of TDM for PSCs.
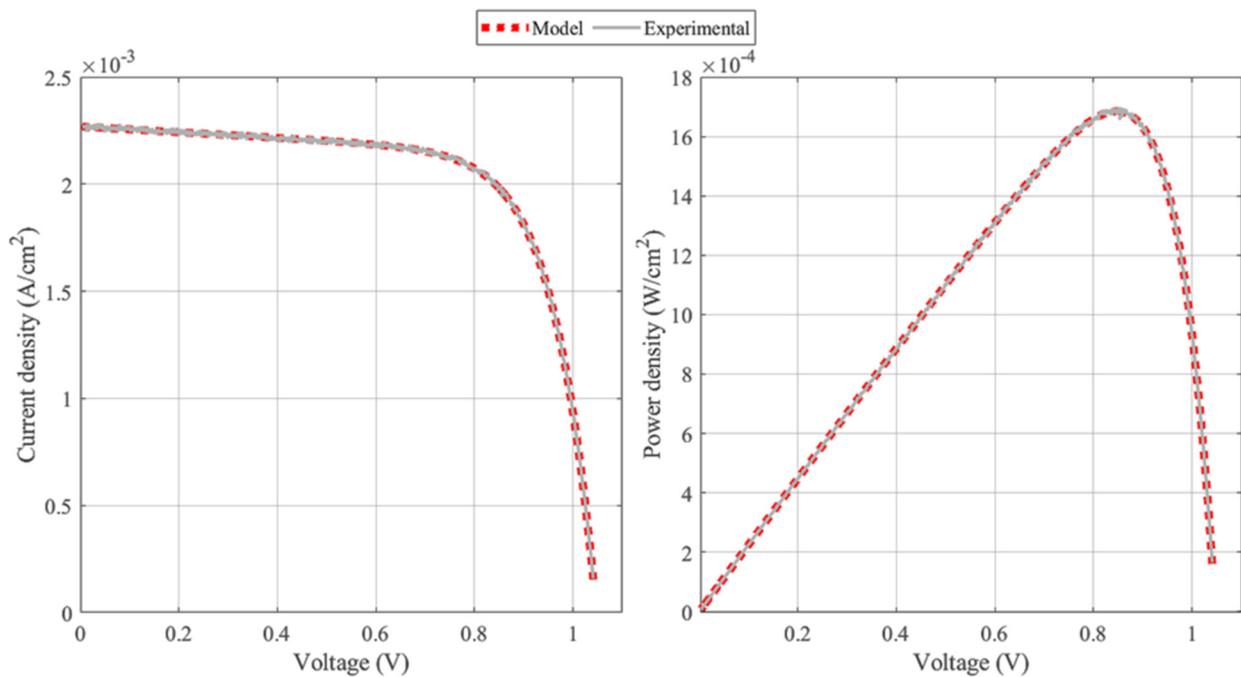

Figure 3. Output characteristic of control PSC using mBES optimizer.
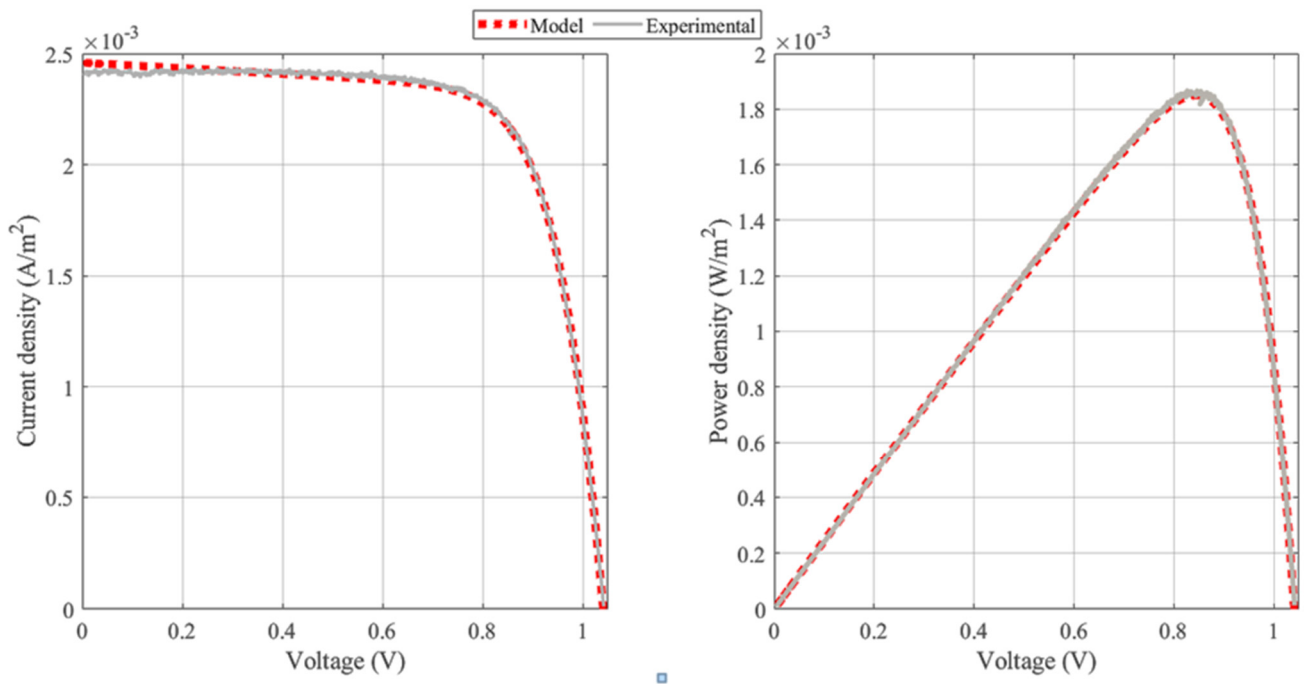
Figure 4. Output characteristic of modified PSC using mBES optimizer.

Figure 5 indicates the convergence curves while applying the different algorithms for both the control and the modified PSCs parameters determination. Based on these figures, the recommended mBES performance is the best in comparison with other used optimizers. Added to that, there is also a fast convergence and lowest cost function when using the proposed mBES optimizer, proving its superiority.
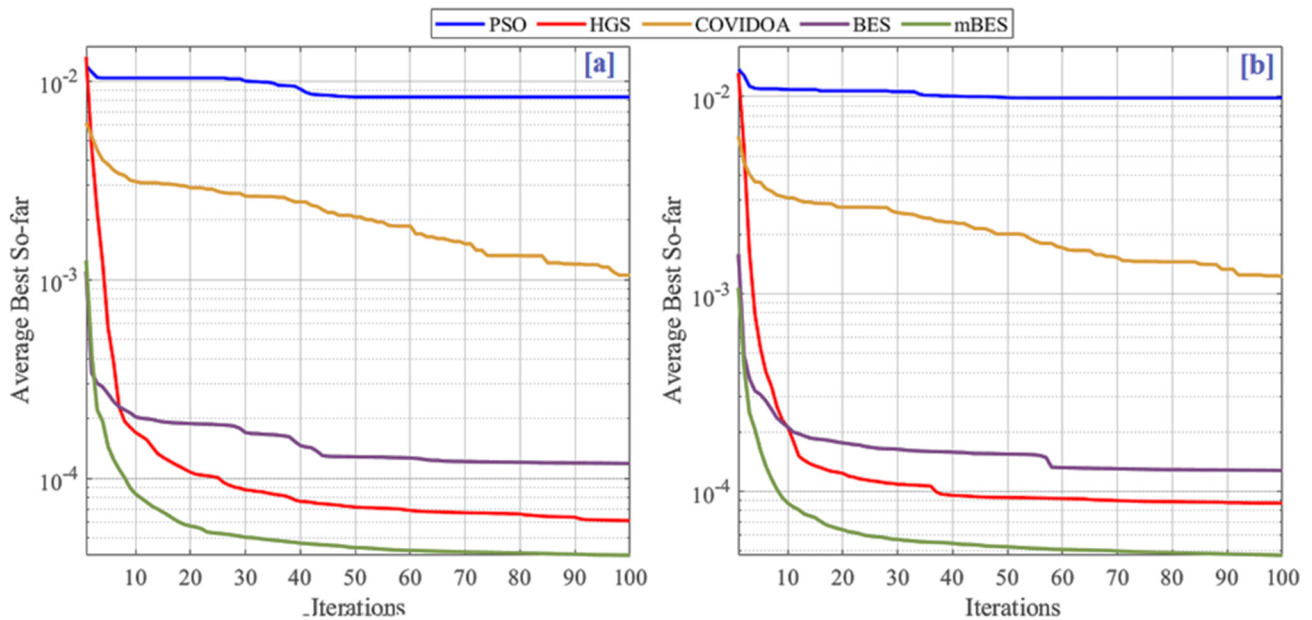

Figure 5. Convergence curves of parameter identification using different algorithms: (**a**) control PSC and (**b**) modified PSC.

Table 5 illustrates the ANOVA test outcomes, while the ranking is presented in Figure 6. The *p*-value is much lower than the F value, suggesting that the reported results disagree.

As demonstrated in Figure 6, the mBES can provide higher mean fitness and variances performance.

Table 5. ANOVA results for control.

Source	SS	df	MS	F	*p*-Value > F
Columns	0.00156	4	0.00039	129.65	7.45117×10^{-47}
Error	0.00044	145	0		
Total	0.002	149			
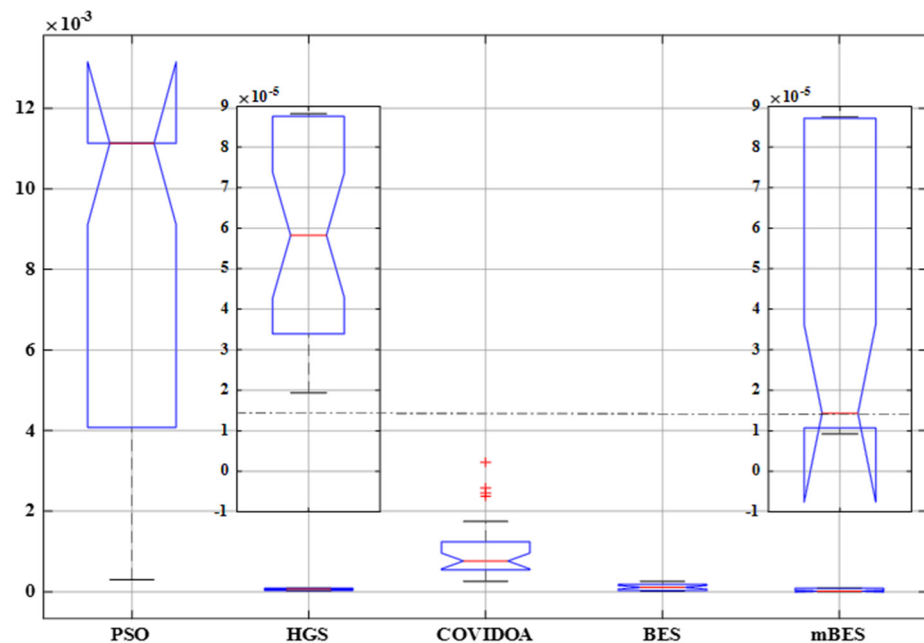
Figure 6. ANOVA ranking for control.

The Tukey HSD (honestly significant difference) examination was used to approve the ANOVA test outcomes after excluding both PSO and COVIDOA due to their limited performances. Figure 7 depicts the results. The mBES has a more excellent mean fitness, indicating that it can tackle this problem successfully. The HGS follows it, then the standard BES.

Analogous to the previous study, the ANOVA test will be accomplished to confirm the performance of each algorithm. The test results are provided in Table 6, and the ranking is displayed in Figure 8. The *p*-value is much smaller than the F value, meaning that the reported results differ. As demonstrated in Figure 8, the mBES can provide higher mean fitness and variances performance. This approves its ability for both types.

Table 6. ANOVA results for control.

Source	SS	df	MS	F	*p*-Value
Columns	0.00218	4	0.00055	259.65	5.39132×10^{-65}
Error	0.00031	145	0		
Total	0.00249	149			
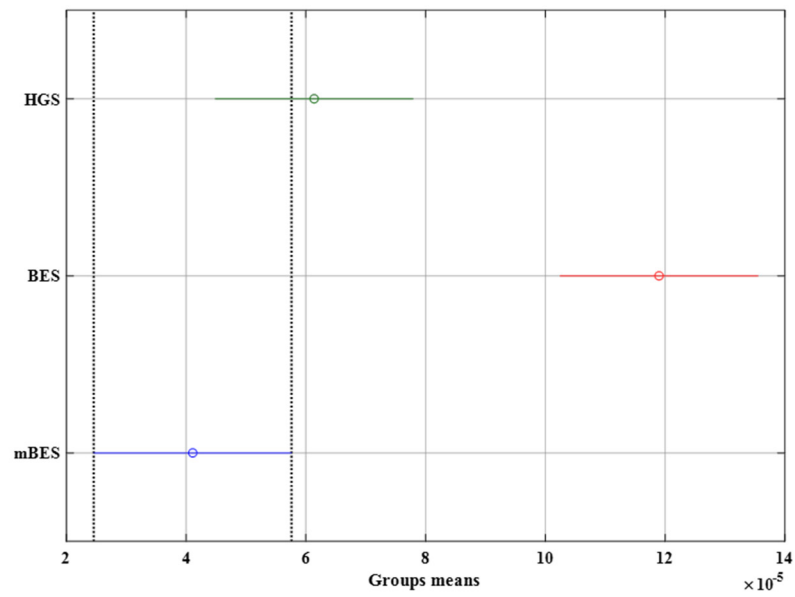
Figure 7. Tukey ranking for control.
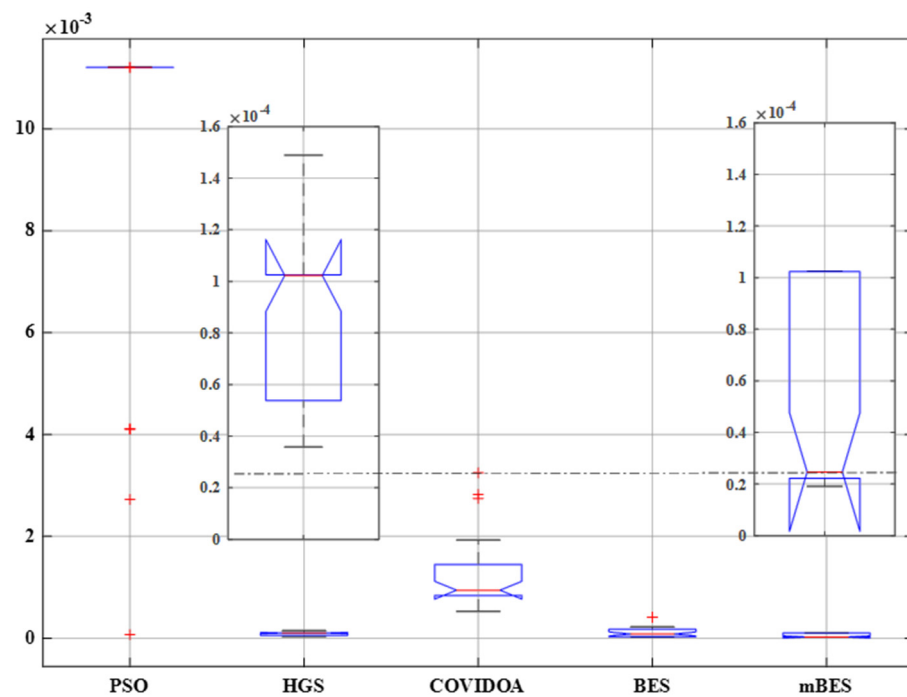
Figure 8. ANOVA ranking for modified.

The Tukey HSD test was performed after excluding both PSO and COVIDAO. Figure 9 depicts the results. The mBES has an excellent mean fitness, indicating that it provides the best performance for both types. The HGS also follows it, then the original BES.
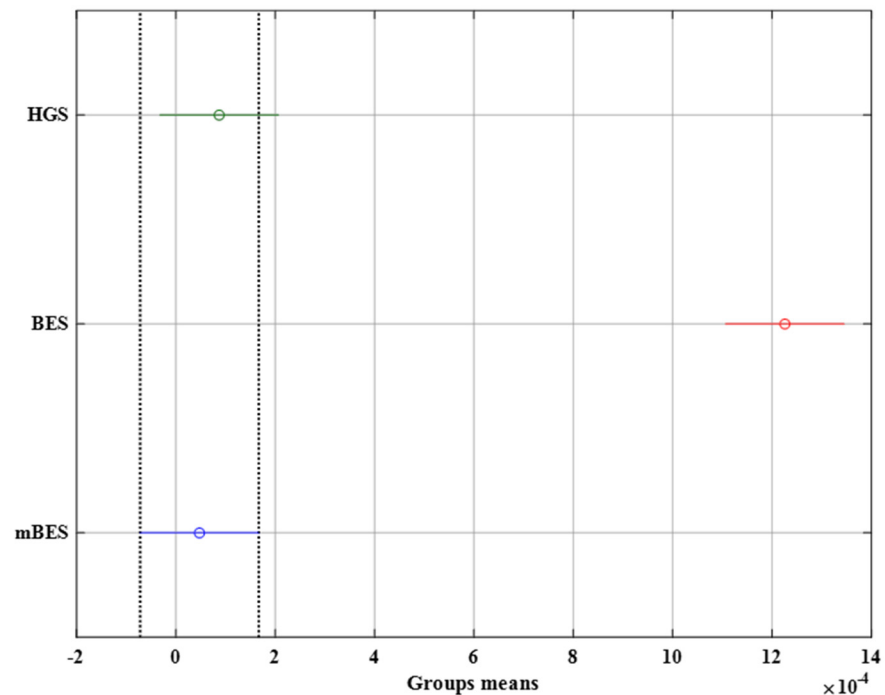
Figure 9. Tukey ranking for modified.

6. Conclusions

In this study, the parameters of perovskite solar cells were determined via a triple diode model solved by a proposed modified bald eagle search algorithm. The results reveal the benefit of the proposed optimizer in assessment with other used optimizers, which are original bald eagle search optimization, particle swarm optimizer, hunger games search, and recent coronavirus disease optimization algorithm. Two experimental datasets were used in this study: the control device and the modified device. The experimental performance was emulated via the triple diode-based model and the proposed optimization algorithm. The results obtained showed a total agreement between the experimental and simulated current density–voltage curves for both control and modified devices at very low deviation values, proving the superiority and the efficient act of the proposed optimization optimizer. The simulation also enables obtaining both the ideality factor of the diode demonstrating the fabrication defects during the manufacture of the device and the diode saturation currents where these elements cannot be obtained experimentally in an easy way, and they are very important in the understanding and analysis of the performance of any solar cell. This study paves the way for future work to determine the third-generation solar cell parameters under dynamic conditions such as partial shading, temperature, and irradiance change.

Author Contributions: Conceptualization, H.R., T.A., A.A.Z., F.F.S. and S.M.A.R.; methodology, A.G.O., H.R., S.M.A.R., S.K.S. and M.A.A.; formal analysis, A.G.O., H.R., T.A., H.M.M., A.A.Z., F.F.S., S.M.A.R., S.K.S. and M.A.A.; investigation, A.G.O., A.A.Z., F.F.S. and M.A.A.; data curation, H.R., T.A. and H.M.M.; writing—original A.G.O., H.R., T.A., H.M.M., A.A.Z., F.F.S., S.M.A.R., S.K.S. and M.A.A.; draft preparation, A.G.O., H.R., T.A., H.M.M., A.A.Z., F.F.S., S.M.A.R., S.K.S. and M.A.A. All authors have read and agreed to the published version of the manuscript.

Data Availability Statement: All data are contained within the article.

Conflicts of Interest: The authors declare no conflict of interest.

References

1. Olabi, A.G.; Obaideen, K.; Elsaid, K.; Wilberforce, T.; Sayed, E.T.; Maghrabie, H.M.; Abdelkareem, M.A. Assessment of the pre-combustion carbon capture contribution into sustainable development goals SDGs using novel indicators. *Renew. Sustain. Energy Rev.* **2022**, *153*, 111710. [CrossRef]
2. Olabi, A.G.; Wilberforce, T.; Elsaid, K.; Sayed, E.T.; Maghrabie, H.M.; Abdelkareem, M.A. Large scale application of carbon capture to process industries—A review. *J. Clean. Prod.* **2022**, *362*, 132300. [CrossRef]
3. Obaideen, K.; Abdelkareem, M.A.; Wilberforce, T.; Elsaid, K.; Sayed, E.T.; Maghrabie, H.M.; Olabi, A.G. Biogas role in achievement of the sustainable development goals: Evaluation, Challenges, and Guidelines. *J. Taiwan Inst. Chem. Eng.* **2022**, *131*, 104207. [CrossRef]
4. Wilberforce, T.; Olabi, A.G.; Sayed, E.T.; Elsaid, K.; Maghrabie, H.M.; Abdelkareem, M.A. A review on zero energy buildings-Pros and cons. *Energy Built Environ.* **2021**, *4*, 25–38. [CrossRef]
5. Obaideen, K.; Nooman AlMallahi, M.; Alami, A.H.; Ramadan, M.; Abdelkareem, M.A.; Shehata, N.; Olabi, A.G. On the contribution of solar energy to sustainable developments goals: Case study on Mohammed bin Rashid Al Maktoum Solar Park. *Int. J.* **2021**, *12*, 100123. [CrossRef]
6. Stranks, S.D.; Eperon, G.E.; Grancini, G.; Menelaou, C.; Alcocer, M.J.P.; Leijtens, T.; Herz, L.M.; Petrozza, A.; Snaith, H.J. Electron-Hole Diffusion Lengths Exceeding 1 Micrometer in an Organometal Trihalide Perovskite Absorber. *Science* **2013**, *342*, 341–344. [CrossRef]
7. Wang, R.; Mujahid, M.; Duan, Y.; Wang, Z.-K.; Xue, J.; Yang, Y. A Review of Perovskites Solar Cell Stability. *Adv. Funct. Mater.* **2019**, *29*, 1808843. [CrossRef]
8. Elsenety, M.M.; Antoniadou, M.; Kaltzoglou, A.; Kontos, A.G.; Philippopoulos, A.I.; Mitsopoulou, C.A.; Falaras, P. Synthesis, characterization of $((CH_3)_3S)_2SnI_6$-nCln and $((CH_3)_3S)_2SnI_6-nBrn$ (n = 1, 2) perovskites and use in dye-sensitized solar cells. *Mater. Chem. Phys.* **2020**, *239*, 122310. [CrossRef]
9. Zaky, A.A.; Christopoulos, E.; Gkini, K.; Arfanis, M.K.; Sygellou, L.; Kaltzoglou, A.; Stergiou, A.; Tagmatarchis, N.; Balis, N.; Falaras, P. Enhancing efficiency and decreasing photocatalytic degradation of perovskite solar cells using a hydrophobic copper-modified titania electron transport layer. *Appl. Catal. B Environ.* **2021**, *284*, 119714. [CrossRef]
10. Elsenety, M.M.; Antoniadou, M.; Balis, N.; Kaltzoglou, A.; Sygellou, L.; Stergiou, A.; Tagmatarchis, N.; Falaras, P. Stability Improvement and Performance Reproducibility Enhancement of Perovskite Solar Cells Following (FA/MA/Cs)PbI3–xBrx/(CH3)3SPbI3 Dimensionality Engineering. *ACS Appl. Energy Mater.* **2020**, *3*, 2465–2477. [CrossRef]
11. Balis, N.; Zaky, A.A.; Perganti, D.; Kaltzoglou, A.; Sygellou, L.; Katsaros, F.; Stergiopoulos, T.; Kontos, A.G.; Falaras, P. Dye Sensitization of Titania Compact Layer for Efficient and Stable Perovskite Solar Cells. *ACS Appl. Energy Mater.* **2018**, *1*, 6161–6171. [CrossRef]
12. Said, A.A.; Xie, J.; Zhang, Q. Recent Progress in Organic Electron Transport Materials in Inverted Perovskite Solar Cells. *Small* **2019**, *15*, 1900854. [CrossRef] [PubMed]
13. Balis, N.; Zaky, A.A.; Athanasekou, C.; Silva, A.M.T.; Sakellis, E.; Vasilopoulou, M.; Stergiopoulos, T.; Kontos, A.G.; Falaras, P. Investigating the role of reduced graphene oxide as a universal additive in planar perovskite solar cells. *J. Photochem. Photobiol. A Chem.* **2020**, *386*, 112141. [CrossRef]
14. Zaky, A.A.; Sehiemy, R.A.E.; Rashwan, Y.I.; Elhossieni, M.A.; Gkini, K.; Kladas, A.; Falaras, P. Optimal Performance Emulation of PSCs using the Elephant Herd Algorithm Associated with Experimental Validation. *ECS J. Solid State Sci. Technol.* **2019**, *8*, Q249. [CrossRef]
15. Conings, B.; Drijkoningen, J.; Gauquelin, N.; Babayigit, A.; D'Haen, J.; D'Olieslaeger, L.; Ethirajan, A.; Verbeeck, J.; Manca, J.; Mosconi, E.; et al. Intrinsic Thermal Instability of Methylammonium Lead Trihalide Perovskite. *Adv. Energy Mater.* **2015**, *5*, 1500477. [CrossRef]
16. Christians, J.A.; Miranda Herrera, P.A.; Kamat, P.V. Transformation of the Excited State and Photovoltaic Efficiency of CH3NH3PbI3 Perovskite upon Controlled Exposure to Humidified Air. *J. Am. Chem. Soc.* **2015**, *137*, 1530–1538. [CrossRef] [PubMed]
17. Zaky, A.A.; Balis, N.; Gkini, K.; Athanasekou, C.; Kaltzoglou, A.; Stergiopoulos, T.; Falaras, P. Dye Engineered Perovskite Solar Cells under Accelerated Thermal Stress and Prolonged Light Exposure. *ChemistrySelect* **2020**, *5*, 4454–4462. [CrossRef]
18. Bencherif, H.; Meddour, F.; Elshorbagy, M.H.; Khalid Hossain, M.; Cuadrado, A.; Abdi, M.A.; Bendib, T.; Kouda, S.; Alda, J. Performance enhancement of $(FAPbI_3)_{1-x}(MAPbBr_3)x$ perovskite solar cell with an optimized design. *Micro Nanostruct.* **2022**, *171*, 207403. [CrossRef]
19. Hossain, M.K.; Arnab, A.A.; Das, R.C.; Hossain, K.M.; Rubel, M.H.K.; Rahman, M.F.; Bencherif, H.; Emetere, M.E.; Mohammed, M.K.A.; Pandey, R. Combined DFT, SCAPS-1D, and wxAMPS frameworks for design optimization of efficient Cs_2BiAgI_6-based perovskite solar cells with different charge transport layers. *RSC Adv.* **2022**, *12*, 35002–35025. [CrossRef]
20. Bencherif, H.; Khalid Hossain, M. Design and numerical investigation of efficient $(FAPbI_3)_{1-x}(CsSnI_3)_x$ perovskite solar cell with optimized performances. *Sol. Energy* **2022**, *248*, 137–148. [CrossRef]
21. Hossain, M.K.; Rubel, M.H.K.; Toki, G.F.I.; Alam, I.; Rahman, M.F.; Bencherif, H. Effect of Various Electron and Hole Transport Layers on the Performance of CsPbI3-Based Perovskite Solar Cells: A Numerical Investigation in DFT, SCAPS-1D, and wxAMPS Frameworks. *ACS Omega* **2022**, *7*, 43210–43230. [CrossRef] [PubMed]

22. Hossain, M.K.; Raihan, G.A.; Akbar, M.A.; Kabir Rubel, M.H.; Ahmed, M.H.; Khan, M.I.; Hossain, S.; Sen, S.K.; Jalal, M.I.E.; El-Denglawey, A. Current Applications and Future Potential of Rare Earth Oxides in Sustainable Nuclear, Radiation, and Energy Devices: A Review. *ACS Appl. Electron. Mater.* **2022**, *4*, 3327–3353. [CrossRef]

23. Hossain, M.K.; Biswas, M.C.; Chanda, R.K.; Rubel, M.H.H.K.; Khan, M.I.; Hashizume, K. A review on experimental and theoretical studies of perovskite barium zirconate proton conductors. *Emergent Mater.* **2021**, *4*, 999–1027. [CrossRef]

24. Nadeem, A.; Sher, H.A.; Murtaza, A.F.; Ahmed, N. Online current-sensorless estimator for PV open circuit voltage and short circuit current. *Sol. Energy* **2021**, *213*, 198–210. [CrossRef]

25. Ismaeel, A.A.K.; Houssein, E.H.; Oliva, D.; Said, M. Gradient-Based Optimizer for Parameter Extraction in Photovoltaic Models. *IEEE Access* **2021**, *9*, 13403–13416. [CrossRef]

26. Allam, D.; Yousri, D.A.; Eteiba, M.B. Parameters extraction of the three diode model for the multi-crystalline solar cell/module using Moth-Flame Optimization Algorithm. *Energy Convers. Manag.* **2016**, *123*, 535–548. [CrossRef]

27. Zaky, A.A.; Fathy, A.; Rezk, H.; Gkini, K.; Falaras, P.; Abaza, A. A Modified Triple-Diode Model Parameters Identification for Perovskite Solar Cells via Nature-Inspired Search Optimization Algorithms. *Sustainability* **2021**, *13*, 12969. [CrossRef]

28. Zaky, A.A.; Ibrahim, M.N.; Taha, I.B.M.; Yousif, B.; Sergeant, P.; Hristoforou, E.; Falaras, P. Perovskite Solar Cells and Thermoelectric Generator Hybrid Array Feeding a Synchronous Reluctance Motor for an Efficient Water Pumping System. *Mathematics* **2022**, *10*, 2417. [CrossRef]

29. Zaky, A.A.; Alhumade, H.; Yousri, D.; Fathy, A.; Rezk, H.; Givalou, L.; Falaras, P. Modeling and Optimization of Triple Diode Model of Dye-Sensitized Solar Panel Using Heterogeneous Marine Predators Algorithm. *Mathematics* **2022**, *10*, 3143. [CrossRef]

30. Zaky, A.A.; Sergeant, P.; Stathatos, E.; Falaras, P.; Ibrahim, M.N. Employing Dye-Sensitized Solar Arrays and Synchronous Reluctance Motors to Improve the Total Cost and Energy Efficiency of Solar Water-Pumping Systems. *Machines* **2022**, *10*, 882. [CrossRef]

31. Abdelrazek, A.S.; El-Sehiemy, R.A.; Rezk, H.; Ghoniem, R.M.; Falaras, P.; Zaky, A.A. Dynamic Electrical Models of Perovskite Solar Cells Considering Hysteresis and Charge Accumulations Effects by Using Equilibrium Optimizer. *IEEE Access* **2022**, *10*, 104111–104122. [CrossRef]

32. Eslami, M.; Akbari, E.; Seyed Sadr, S.T.; Ibrahim, B.F. A novel hybrid algorithm based on rat swarm optimization and pattern search for parameter extraction of solar photovoltaic models. *Energy Sci. Eng.* **2022**, *10*, 2689–2713. [CrossRef]

33. Noroozi, M.; Mohammadi, H.; Efatinasab, E.; Lashgari, A.; Eslami, M.; Khan, B. Golden Search Optimization Algorithm. *IEEE Access* **2022**, *10*, 37515–37532. [CrossRef]

34. Yaghoubi, M.; Eslami, M.; Noroozi, M.; Mohammadi, H.; Kamari, O.; Palani, S. Modified Salp Swarm Optimization for Parameter Estimation of Solar PV Models. *IEEE Access* **2022**, *10*, 110181–110194. [CrossRef]

35. Eslami, M.; Shareef, H.; Mohamed, A.; Khajehzadeh, M. Damping controller design for power system oscillations using hybrid GA-SQP. *Int. Rev. Electr. Eng.* **2011**, *6*, 888–896.

36. Khajehzadeh, M.; Taha, M.R.; Eslami, M. Opposition-based firefly algorithm for earth slope stability evaluation. *China Ocean. Eng.* **2014**, *28*, 713–724. [CrossRef]

37. Eslami, M.; Neshat, M.; Khalid, S.A. A Novel Hybrid Sine Cosine Algorithm and Pattern Search for Optimal Coordination of Power System Damping Controllers. *Sustainability* **2022**, *14*, 541. [CrossRef]

38. Khajehzadeh, M.; Keawsawasvong, S.; Nehdi, M.L. Effective Hybrid Soft Computing Approach for Optimum Design of Shallow Foundations. *Sustainability* **2022**, *14*, 1847. [CrossRef]

39. Gkini, K.; Balis, N.; Papadakis, M.; Verykios, A.; Skoulikidou, M.-C.; Drivas, C.; Kennou, S.; Golomb, M.; Walsh, A.; Coutsolelos, A.G.; et al. Manganese Porphyrin Interface Engineering in Perovskite Solar Cells. *ACS Appl. Energy Mater.* **2020**, *3*, 7353–7363. [CrossRef]

40. Ferahtia, S.; Rezk, H.; Djerioui, A.; Houari, A.; Motahhir, S.; Zeghlache, S. Modified bald eagle search algorithm for lithium-ion battery model parameters extraction. *ISA Trans.* **2022**, *in press*. [CrossRef]